Miniaturized tunable extended eight-port hybrid coupler for 1.5 T MRI

Zachary A. Colwell [ID] and Sung-Min Sohn [ID]

School of Biological and Health System Engineering, Arizona State University, Tempe, Arizona, USA

Abstract

This paper presents a miniaturized, tunable, high-power, eight-port hybrid coupler, based on a lumped element hybrid coupler topology. The 90° hybrid couplers are ubiquitous elements used for feeding RF coils in quadrature in magnetic resonance imaging (MRI) systems. Due to the low Larmor frequency (64 MHz) of 1.5 T MRI, distributed elements are too large for practical circuits to drive multi-port RF coils. Thus, miniaturization with MRI-compatible, non-magnetic, and high-power components is necessary. First, a miniaturized hybrid coupler is proposed for MRI systems with non-magnetic variable capacitors. Afterwards, the miniaturization methodology is applied to develop an eight-port coupler, capable of supporting both a transmit and a receive quadrature RF coil system. The high-power (up to 1 kilowatt) extended coupler measures 10 cm × 6 cm. Test results show that each port has a return loss of more than 16 dB, each input-isolated port is isolated by more than 24 dB, and each output has an insertion loss of less than 2.5 dB and output phases of 0.0°, 90.8°, 182.1°, and 278.7°.

CAMBRIDGE UNIVERSITY PRESS

Introduction

The operating frequency of magnetic resonance imaging (MRI) scanners, known as the Larmor frequency, is dependent on the magnetic field strength. MRI operates by applying a large (> 0.5 T) static magnetic field (B_0) to a patient, resulting in the nuclear precession of hydrogen in the body. If another local RF magnetic field (B_1) is excited, through an RF pulse, orthogonally to the B_0 field, at the Larmor frequency, the equilibrium of precession is temporarily disturbed. Once the pulse stops, the nuclei re-establish equilibrium and emit an RF signal at the Larmor frequency. This signal, denoted as the "MR signal" is received via RF coils for image reconstruction by the MRI console. Various types of RF coils have been developed over MRI's lifetime. Until the 1990s, linear surface coils dominated the industry until it was shown that circularly polarized "quadrature" coils increase the signal to noise ratio (SNR) and waste less RF power [1].

A linearly polarized magnetic field can be deconstructed into two circularly polarized, counterrotating magnetic fields; for MRI, one component is chosen to rotate with the nuclear precession, while the other rotates opposite of nuclear precession. For a single linear RF coil, the component rotating opposite to nuclear precession is not received as a signal, rather, it is dissipated as heat. To combat this signal loss, quadrature coil systems were developed. Quadrature coils systems operate by placing two linear coils orthogonally to one another and feeding them with a 90° phase difference [2]. This is readily achieved with simple RF loop coils and a hybrid coupler. A further SNR improvement of $\sqrt{2}$ can be obtained with the quadrature coils [3].

With 1.5 T MRI machines, the Larmor frequency of hydrogen nuclei is 64 MHz, even when designing circuits on the common FR4 substrate ($\varepsilon_r = 4.5$), the wavelength is ~221 cm. Thus, for practical use, classically distributed RF circuits, such as hybrid couplers, must be miniaturized. Since the level of RF transmit power is a few hundreds of watts to a kilowatt to excite protons inside the human body, a hybrid coupler with high power capability is also necessary.

Systems with multiple quadrature coil pairs require multiple hybrid couplers, demanding more circuits and more cables to be interfaced with the MRI system. Multiple bulky couplers and their cables are not readily integrated into coil frames. This also makes coil impedance matching more difficult, since the cables and circuits, themselves, can become a sensitive component of the radiative element, thus degrading coil performance.

This paper seeks to introduce a straightforward methodology for developing a miniaturized extended coupler with eight RF ports dedicated to MRI applications. This extended coupler is to be integrated with systems containing both quadrature-transmit and quadrature-receive coils. First, 90° and 180° hybrid couplers are miniaturized with lumped elements. Then, these topologies are brought together to form the extended coupler.

Each MRI machine's Larmor frequency is different (by up to a few 100's of kHz) and varies slightly day-to-day. The loading effect, due to the subject lying in the near field of the RF coils, also changes the coil systems' impedance matching conditions [4]. Thus, narrowband
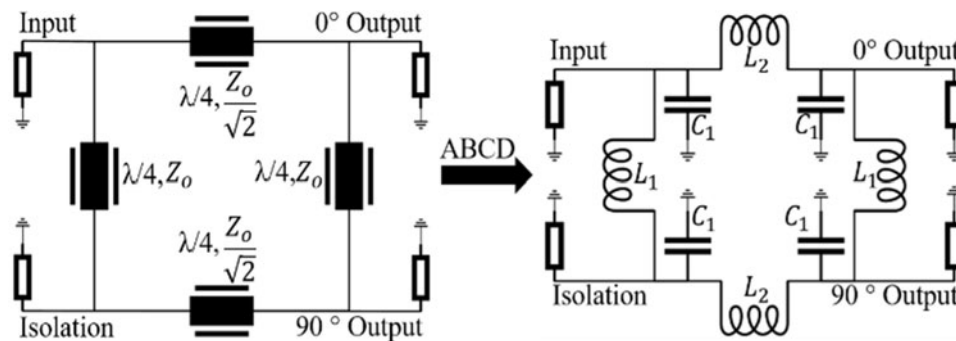
Fig. 1. A 90° hybrid coupler ABCD transformation.

tunability, via high-power and variable non-magnetic capacitors, is attractive to optimize the coupler's performance for each unique imaging study.

Hybrid coupler design method

The 90° hybrid couplers are four-port RF circuits with one input port, one isolation port, and two equal power split (−3 dB) output ports with a 90° phase difference. They are easily designed with four quarter wavelength ($\lambda/4$) transmission lines, two with characteristic impedance Z_o Ω and two with characteristic impedance $\frac{Z_o}{\sqrt{2}}$ Ω, as shown in Fig. 1 [5]. At 64 MHz, a manufacturing process using FR4 requires transmission lines with a length of more than 55 cm, rendering them impractical to manufacture. Reducing these transmission lines to lumped element equivalents is paramount. Reducing a transmission line of any length and impedance to lumped components is readily performed with the use of ABCD matrices. For this design, $\lambda/4$ transmission lines with characteristic impedances of 50 Ω (Z_o) and $\frac{50}{\sqrt{2}}$ Ω ($\frac{Z_o}{\sqrt{2}}$) are reduced to a series inductor placed in-between two shunt capacitors. The ABCD matrix setup is as follows:

$$\begin{bmatrix} \cos(\beta l) & jZ\sin(\beta l) \\ jY\sin(\beta l) & \cos(\beta l) \end{bmatrix}_{90°} = \begin{bmatrix} 1 & 0 \\ Y_C & 1 \end{bmatrix}\begin{bmatrix} 1 & Z_L \\ 0 & 1 \end{bmatrix}\begin{bmatrix} 1 & 0 \\ Y_C & 1 \end{bmatrix},$$

(1)

where l is the length of the transmission line, β is equal to $2\pi/\lambda$, λ is the wavelength at 64 MHz using FR4, Z is the transmission line impedance, Y is the transmission line admittance, Y_C is the capacitor admittance, and Z_L is the inductor impedance. Solving for C and L in terms of their admittance and impedance, respectively, results in:

$$C_{Z_o} = 49.735 \text{ pF}, \quad C_{\frac{Z_o}{\sqrt{2}}} = 70.337 \text{ pF},$$

$$L_{Z_o} = L_1 = 124.339 \text{ nH}, \quad \text{and } L_{\frac{Z_o}{\sqrt{2}}} = L_2 = 87.922 \text{ nH}.$$

For building and tuning convenience, the capacitors within 2 cm of each other were approximated as being in parallel. This results in four capacitors with values $C_1 = 120.072$ pF. The 180° hybrid coupler design follows the same methodology but with three $\lambda/4$ transmission lines and one $3\lambda/4$ transmission line, all with a characteristic impedance $\sqrt{2}Z_o$ Ω. The longer transmission line is unable to be replaced with a series inductor and shunt capacitors, rather, it requires a series capacitor with two shunt inductors, as seen in Fig. 2.

The extended coupler

The extended coupler is an eight-port RF circuit based on the aforementioned hybrid coupler topologies. By merging one 90° hybrid coupler with two 180° hybrid couplers, a device with one input port, one isolation port, two MRI console receive ports, and four output ports with an equal power split (−6 dB) and with 0°, 90°, 180°, and 270° of phase is acquired.

The extended coupler schematic can be seen in Fig. 2, where the dashed blue line contains the single 90° hybrid coupler and the two solid red lines contain the two 180° hybrid couplers. There exists one shared capacitor between the 90° hybrid coupler and each 180° hybrid coupler, noted as $C_4 = 155.241$ pF. A summary of the component values used in the fabricated extended coupler design can be found in Table 1. C_2 and C_2^*, as well as C_3 and C_3^*, were calculated to be the same value, but tuned differently for the physical circuit.

Many MRI systems contain a single volume transmit coil to increase B_1 field uniformity and multiple surface receive coils to increase MR signal reception [6, 7]. Such systems can support multiple receive ports but only a single transmit port, unless the transmit signal is divided amongst multiple coils.

The extended coupler accommodates such systems by supplying the transmit signal from console to input, hence it is split between Tx_1 and Tx_2, which connect to the transmit volume coil with a 90° phase difference. The surface receive coils directly connect to Rx_1 and Rx_2, which are coupled to Rx_1 output and Rx_2 output, also with a 90° phase difference. These receive output ports connect to the MRI console for image reconstruction. Finally, isolation is terminated.

Isolating the transmit signal input and the receive channel output from each other is a defining characteristic of standard MRI couplers. Due to the isolation properties of the embedded hybrid couplers, the extended coupler input is isolated from "isolation", "Rx_1 output", and "Rx_2 output", highlighting how the extended coupler is an extension of the already well-understood hybrid coupler for MRI systems.

Coupler fabrication

For the physical circuit, FR4 ($\varepsilon_r = 4.5$) coplanar waveguides with 1.36 mm trace width, 1 mm thickness, and 0.4 mm separation gap from trace to ground were manufactured to connect lumped elements. The extended coupler measures only 6 cm × 10 cm since it assumes variable capacitors can be soldered on top of the static capacitors, thus saving circuit area. The MRI console supplies high-power pulse sequences and the bore is highly magnetic,
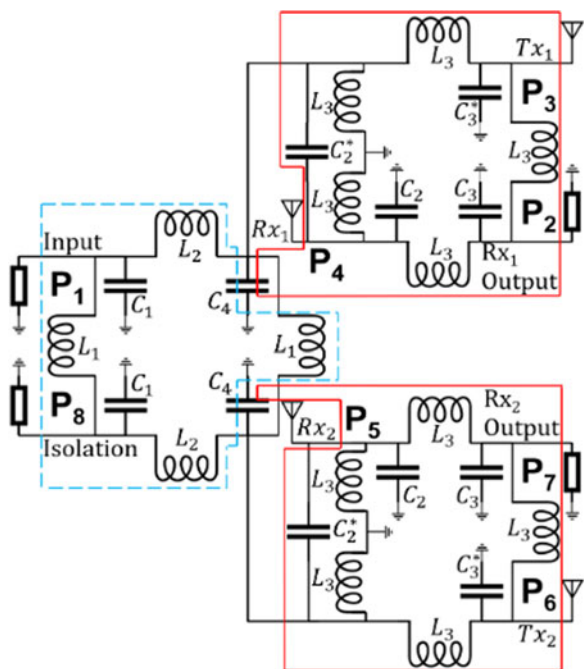
Fig. 2. Extended coupler schematic.

Table 1. Fabricated extended coupler component values

Component	Calculated value	Physical value	Extra tunable range
C_1	120.072 pF	121 pF	NA
C_2	35.169 pF	48 pF	NA
C_2^*	35.169 pF	24 pF	+1 to 16 pF
C_3	70.337 pF	75 pF	NA
C_3^*	70.337 pF	62 pF	+1 to 16 pF
C_4	155.241 pF	150 pF	NA
L_1	124.339 nH	110 nH	NA
L_2	87.992 nH	82 nH	NA
L_3	175.843 nH	180 nH	NA

therefore high-power and non-magnetic components must be used. The variable capacitors (Knowles Voltronics) have a tunable range from 1 to 16 pF with the voltage rating of 750 V, the fixed capacitors (Knowles Syfer) can handle a 3.6 kV continuous wave signal, the inductors (Coilcraft) can support up to 5 A of current, and the trace widths can conduct 5 A of current with an assumed temperature increase to 60°C. All connectors also are non-magnetic, as tested in the bore of a 1.5 T MRI machine.

The physical circuit can be seen in Fig. 3. The ports are numbered as follows: 1 – input, 2 – Rx_1 output, 3 – $Tx_1(0°)$, 4 – $Rx_1(180°)$, 5 – $Rx_2(270°)$, 6 – $Tx_2(90°)$, 7 – Rx_2 output, and 8 – isolation.

Results

The extended coupler was simulated with Keysight's ADS. The real value of the inductors physically used was substituted into the ADS circuit before tuning the capacitors to optimize the
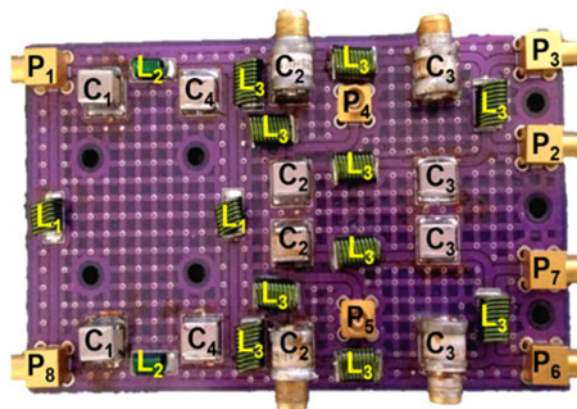
Fig. 3. Extended coupler physical circuit.

circuit. All measurements were collected using a four-port vector network analyzer (Keysight 9370A) as shown in Fig. 4.

Simulation and measured data can be found in Fig. 5, where the horizontal axis of each plot is frequency, from 50 to 80 MHz and the vertical axes are return loss (dB), coupling (dB), and phase (degrees), respectively. All dashed line plots represent simulation data, whereas solid line plots represent test bench data.

The plot in Fig. 5(a) shows the measured return loss of each port to be at least 16 dB. Seen in Fig. 5(b) plot is the coupling between input (P_1) and Tx_1 (P_3), Tx_2 (P_6), Rx_1 (P_4), and Rx_2 (P_5) in dB. All bench plots (solid lines) are below 8.5 dB (2.5 dB above the minimum 6 dB). In Fig. 5(c) plot is the phase of the Tx_1, Tx_2, Rx_1, and Rx_2. The output phase bench data (solid lines) follow nearly the exact distribution as the simulation data (dashed line) with phase measurements of 0.0°, 90.8°, 182.1°, and 278.7° at 64 MHz. The decoupling between input and isolation (P_8), between input and Rx_1 output (P_2), and between input and Rx_2 output (P_7) are all greater than 24 dB. Since all of the ports are well isolated, and four of the ports are orthogonal outputs, a secondary application of this circuit can be found by exciting the input port and terminating three ports (Rx_1 output, Rx_1 output, and isolation) instead of just one. Thus, the circuit can also be used as an orthogonal power divider with 0.0°, 90.8°, 182.1°, and 278.7° outputs.

When designing circuits like a hybrid coupler, physical symmetry is a convenience for fast and reasonably accurate design. The extended coupler's line of symmetry is clearly seen about its horizontal axis, where, for example, the assumption is made that $L_{2, top}$ and $L_{2, bottom}$ are equal. Real inductors and capacitors, however, have tolerances. All components used in the extended coupler are rated for a 5% tolerance. To account for the discrepancies between the simulated and measured data, a Monte Carlo analysis was performed. Each component was varied, in simulation, within ±5% of its nominal value. The tunable capacitors were not included, since they exist physically to compensate for such discrepancies. The results of the Monte Carlo analysis demonstrated that S_{61} could be in the range of 72°–109°, S_{41} could be in the range of 172°–185°, and S_{51} could be in the range of 250°–287°. These large ranges of output phase highlight the importance of the tunable capacitors for optimizing circuit performance.

Conclusion

Demonstrated in this paper was a straightforward methodology for developing a miniaturized *extended coupler* circuit with high-
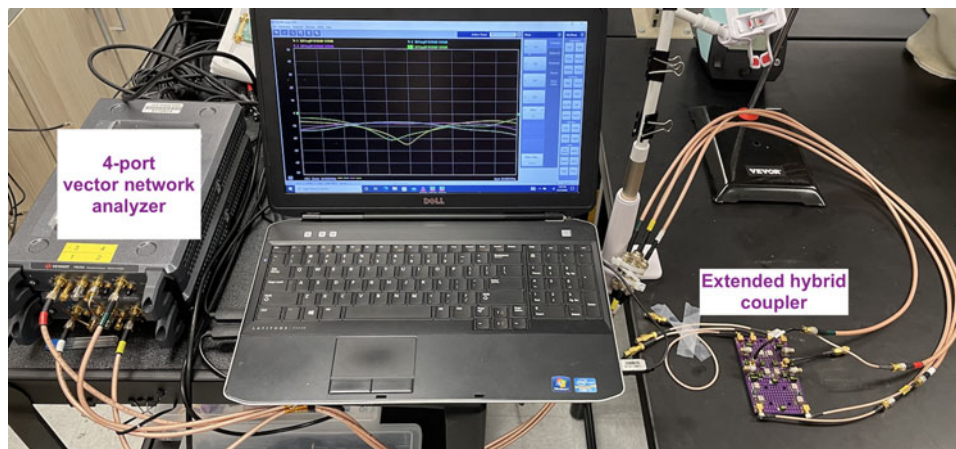
Fig. 4. Test setup with four-port vector network analyzer.
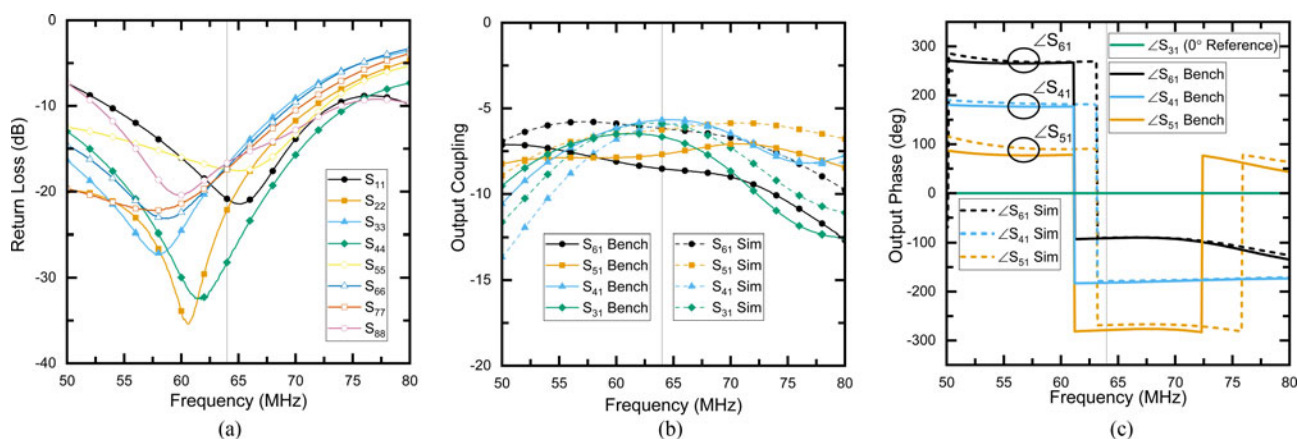
Fig. 5. Extended coupler simulation and bench data. (a) Measured return loss. (b) Coupling factors. (c) Phase shift.

power, non-magnetic lumped elements for 1.5 T MRI. The extended coupler applies to a system which uses two quadrature coil pairs; one for transmit and one for receive. Due to the small size, this extended coupler can be readily integrated into a transceiver coil frame. The coupler performs well with high return loss (>16 dB), high isolation (24 dB), minimal insertion loss (<2.5 dB) to the coil ports, and quadrature phase shifting of 90.8°, 182.1°, and 278.7°. Included in the design are four tunable capacitors to introduce narrowband tunability to compensate for coil loading, daily MRI machine Larmor frequency variation, and lumped element tolerances. A secondary application of this circuit is as an "orthogonal RF power divider" such that one port is excited, three ports are terminated, and the other four ports are well isolated and orthogonal (0.0°, 90.8°, 182.1°, and 278.7°) outputs.

Conflict of interest. The authors declare that they have no known competing financial interests or personal relationship that influenced the work reported in this paper.

References

1. **Glover GH, Hayes CE, Pelc NJ, Edelstein WA, Mueller OM, Hart HR, Hardy CJ, O'Donnell M and Barber WD** (1985) Comparison of linear and circular polarization for magnetic resonance imaging. *Journal of Magnetic Resonance (1969)* **64**, 255–270.
2. **Hyde JS, Jesmanowicz A, Grist TM, Froncisz W and Kneeland JB** (1987) Quadrature detection surface coil. *Magnetic Resonance in Medicine* **4**, 179–184.
3. **Chen CN, Hoult DI and Sank VJ** (1983) Quadrature detection coils – a further $\sqrt{2}$ improvement in sensitivity. *Journal of Magnetic Resonance (1969)* **54**, 324–327.
4. **Sohn SM, DelaBarre L, Vaughan JT and Gopinath A** (2013) 8-channel RF head coil of MRI with automatic tuning and matching. *IEEE MTT-S International Microwave Symposium Digest* **2**, 8–10.
5. **Pozar DM** (2011) *Microwave Engineering*, 4th Edn. Hoboken, NJ: Wiley Global Education.
6. **Hayes CE, Edelstein WA, Schenck JF, Mueller OM and Eash M** (1985) An efficient, highly homogeneous radiofrequency coil for whole-body NMR imaging at 1.5 T. *Journal of Magnetic Resonance* **63**, 622–628.
7. **Gruber B, Froeling M, Leiner T and Klomp DWJ** (2018) RF coils: a practical guide for nonphysicists. *Journal of Magnetic Resonance Imaging: JMRI* **48**, 590–604.

Zachary A. Colwell received Bachelor's and Master's degrees in Electrical Engineering from Arizona State University, Tempe, Arizona, in 2017 and 2018, respectively. He is currently pursuing his Ph.D. in Electrical Engineering in the Bioinspired Circuits and Systems lab at Arizona State University. His current research interests are RF hardware and electronics for MRI applications, particularly, low-power electronics for simultaneous transmit and receive (STAR) systems.

Sung-Min Sohn received Bachelor's and Master's degrees from Korea University, Seoul, South Korea, in 2002 and 2004, respectively, and his Ph.D. from the Department of Electrical and Computer Engineering at the University of Minnesota, Minneapolis, in 2013. From 2004 to 2007, he worked as a circuit design engineer in the analog and mixed signal circuit group, LG Electronics, Seoul, Korea. From 2013 to 2018, he worked at the Center for Magnetic Resonance Research (CMRR) at the University of Minnesota as a postdoctoral fellow, research associate, and research assistant professor. In 2018, he joined the School of Biological and Health System Engineering at Arizona State University. His current research interests include bio-inspired RF/analog/digital circuits and systems. For now, major research topic lies in RF/analog electronics, novel RF coils, and interfaces in magnetic resonance imaging (MRI).